ChemComm

Chemical Communications

rsc.li/chemcomm
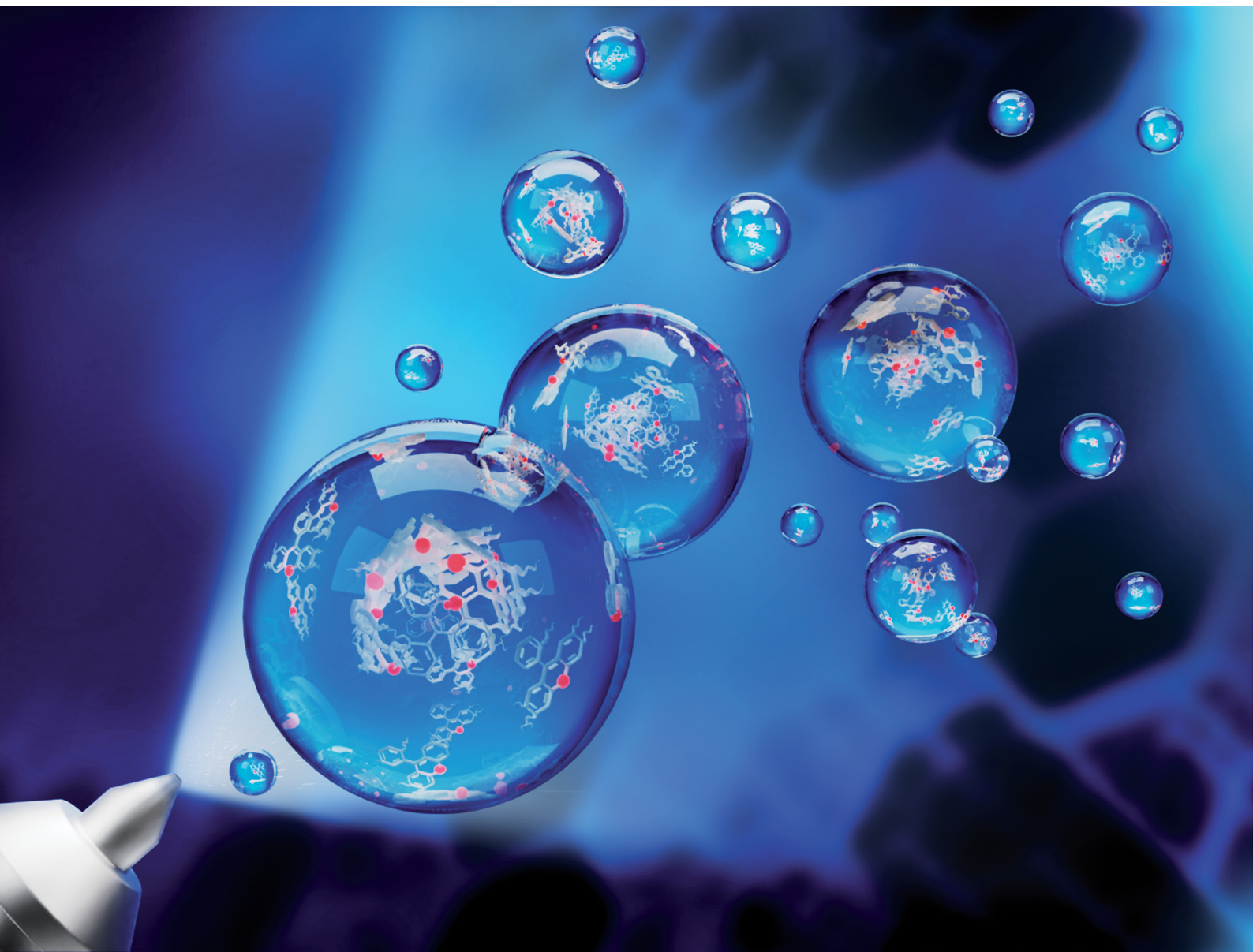
ROYAL SOCIETY
OF CHEMISTRY

COMMUNICATION
Thalappil Pradeep *et al.*
Aggregation of molecules is controlled in microdroplets

Check for updates

Aggregation of molecules is controlled in microdroplets†

Pallab Basuri,‡[a] Jenifer Shantha Kumar,‡[a] Keerthana Unni,[a] Sujan Manna[a] and Thalappil Pradeep [ID] *[ab]

Molecular de-aggregation was observed at the air/water interface of aqueous microdroplets. We probed this phenomenon using dyes such as Rhodamine 6G (R6G), Rhodamine B, acridine orange, and fluorescein, which show aggregation-induced shift in fluorescence. The fluorescence micrographs of microdroplets derived from the aqueous solutions of these dyes show that they are monomeric at the air/water interface, but highly aggregated at the core. We propose that rapid evaporation of the solvent influences the de-aggregation of molecules at the air–water interface of the microdroplets.

The behaviour of molecules in a confined volume is distinctly different compared to those present in bulk liquids.[1] This is evident from several microdroplet studies where molecules show accelerated reaction kinetics,[2,3] restricted rotation,[4] spatial localization,[5] spontaneous oxidation–reduction,[6–11] and partial solvation.[12,13] These contribute to interfacial electric fields[14] and extraordinary pH changes[15,16] in microdroplets. Such microdroplets are generated usually using electrospray and pneumatic spray and less commonly by effects such as Leidenfrost, acoustic levitation and trapping on hydrophobic surfaces. Nevertheless, most of these phenomena occur at the gas–liquid interface of the droplets. These properties were understood mainly by mass spectrometry or by in-droplet molecular spectroscopy. Very few studies involved imaging of microdroplets to probe such extraordinary properties of molecules. For example, the Cooks group used a super-resolution Nikon Ti-E microscope for 3D structured illumination microscopy (SIM) to image Rhodamine B containing microdroplets created by nano-electrospray ionization (nESI).[17] The authors found that the acceleration of reactions in microdroplets is strongly associated with processes at their

gas–liquid interfaces. The Zare group used microscopy to image deposited droplets on a glass surface created by nebulized ESI and observed the same phenomenon.[18] Very recently, they reported spatial localization of charged molecules in water-in-oil microdroplets using fluorescence microscopy.[5] Our recent investigation using nanoparticles showed anisotropic particle distribution in microdroplets along with the observation of microvacuoles at the interior of the droplets.[19] However, this subject is still lacking critical information on the properties of molecules present in small volumes.

Dye molecules such as R6G, Rhodamine B, acridine orange, *etc.* show emission spectral shift induced by molecular aggregation, which is used as a measure of local concentrations.[20] The R6G emission peak maximum shows a redshift and a reduction in fluorescence quantum yield due to polymerization at higher concentrations.[21,22] The dimerization of cationic R6G could occur in two ways, such as head-to-head and head-to-tail denoted as H and J aggregates, respectively.[23,24] It should be noted that the extent of aggregation and the corresponding molecular structure can also be controlled by parameters such as temperature,[25] light,[26] addition of ionic or macromolecular species,[27] and solvent polarity.[28]

Herein, we used a combined approach involving (i) aggregation-induced emission (AIE), (ii) emission spectral shift (ESS), and (iii) fluorescence quenching of dye molecules to have an in-depth understanding of molecular behaviour in microdroplets. Fluorescence microscopy was utilized to image microdroplets. A few factors such as the droplet traveling distance, nebulization gas pressure, potential, and pH of the solution have been varied, and their effects have been documented.

We observed that solid R6G, a dark red powder, shows no luminescence owing to its highly aggregated state. A photograph of R6G powder taken on a Petri dish under visible light is shown in Fig. 1a. But 100 μM R6G solution exhibits red colour in visible light and is bright yellow in UV light (Fig. 1b). However, when 0.1 μL of the same 100 μM solution was dropcast on a glass slide and allowed to dry, we observed bright red emission (Fig. 1c). This shows that the dropcast thin-film induces aggregation in comparison to the solution state

[a] *DST Unit of Nanoscience (DST UNS), Thematic Unit of Excellence (TUE), Department of Chemistry, Indian Institute of Technology Madras, Chennai 600036, India. E-mail: pradeep@iitm.ac.in*

[b] *International Centre for Clean Water, Chennai, Tamil Nadu 600113, India*
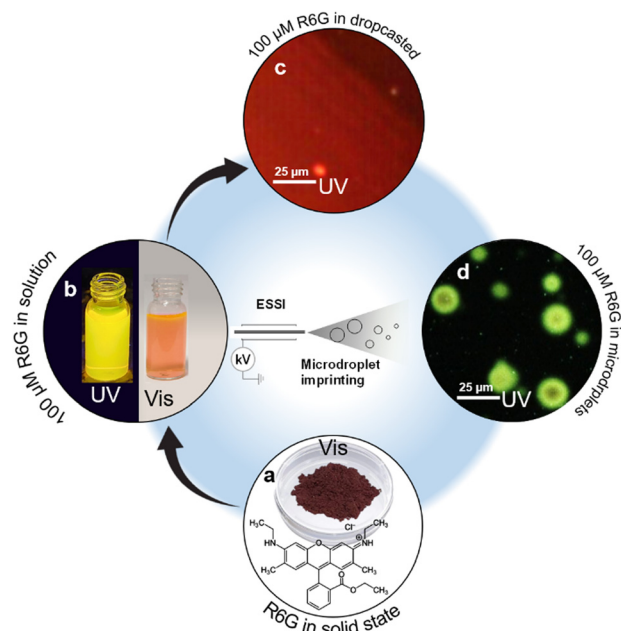
‡ These authors contributed equally.

Fig. 1 Different states of R6G under visible and UV light. (a) R6G in the powder form is dark red under visible light and shows no luminescence under UV light. The inset shows the molecular structure of R6G. (b) An aqueous R6G solution of 100 μM concentration. (c) 0.1 μL dropcast of the same solution on a clean glass slide for fluorescence microscopy. (d) Fluorescence microscopy image of imprinted microdroplets generated from a 100 μM solution using an ESSI source, as shown schematically in the inset, at the centre of the image. The scale bar is 25 μm. UV illumination was applied using a DAPI (4′,6-diamidino-2-phenylindole) filter for (c) and (d).

(Fig. S3, ESI†). Note that, in bulk solution, the solvation helps to restrict molecular aggregation, and as a result we observed yellow luminescence. However, molecules form aggregates in the film to reduce the overall energy, which eventually redshifts the emission. Surprisingly, when the same solution was electro-sprayed and the droplets were imprinted on a glass slide (see experimental details, Fig. S1 in the ESI†), we observed green luminescence (Fig. 1d). The experimental details and a schematic representation of droplet imaging by fluorescence microscopy are presented in the ESI† (Fig. S1 and S2, ESI†). This suggests that molecules are likely to de-aggregate and become monomeric in microdroplets. Such a drastic difference between the solution phase, dropcast solid thin film, and imprinted microdroplets encouraged us to investigate the effect further and its dependence on the other parameters of droplet generation. The detailed mechanism of de-aggregation at the interface is not clear at present. We suggest that the fast evaporation of the solvent at the dynamic interface and the relatively slow movement of large non-volatile dye molecules result in de-aggregation. To verify this, we generated microdroplets with a solvent of different volatility. Fig. S4 (ESI†) shows the fluorescence images of water and methanol microdroplets containing R6G, imprinted on glass slides. We observed that the dye molecules in methanol droplets (Fig. S4a, ESI†) are completely monomeric in nature, whereas the water microdroplets (Fig. S4b, ESI†) show the monomeric form predominantly at the interface and are aggregated at the interior.

The tip-to-inlet distance plays an important role in determining the chemistry of the molecules in microdroplets.[17] We observed that the degree of de-aggregation increased with increasing distance. Fig. 2a displays a schematic diagram of the variable distance droplet deposition setup. The fluorescence images of droplets at 0.3, 1.5, and 3 cm distances are shown in Fig. 2b–d. Interestingly, the droplets sprayed from a distance of 0.3 cm show predominantly red luminescence at the interior and green luminescence towards the periphery. Notably, the red colour at the interior of the droplet is dull in comparison to the dropcast sample shown in Fig. 1c. We suggest that the droplet core exhibited a higher order of aggregation than that of the dropcast sample. Also, microdroplets induce fluorescence quenching at the core. The droplets, allowed to travel a 1.5 cm distance, showed red and green colours at the core and green emission towards the periphery. Further increase of the travel distance to 3 cm led to higher de-aggregation of the dye leading to green emission throughout the droplet (Fig. 2d). The spray distance is known to affect the size of the droplets. These observations suggest that the core of the droplets at shorter distances exhibits bulk-like properties, resulting in AIE in the red region. The longer the droplet travels, the more the de-aggregated dye molecules form which appeared green. This shows that the droplets at a 1.5 cm spray distance may be at an intermediate state, showing a mixed composition of aggregated and de-aggregated dye molecules. Previous reports on droplet imaging show that the imprinting of droplets on a solid surface retains the spatial distribution of molecules in the droplets and reliably reflects the nature of droplets in the electrospray.[29,30]

Similar to the distance effect, it was observed that the nebulization gas pressure also affected the aggregation/de-aggregation dynamics of R6G molecules significantly.
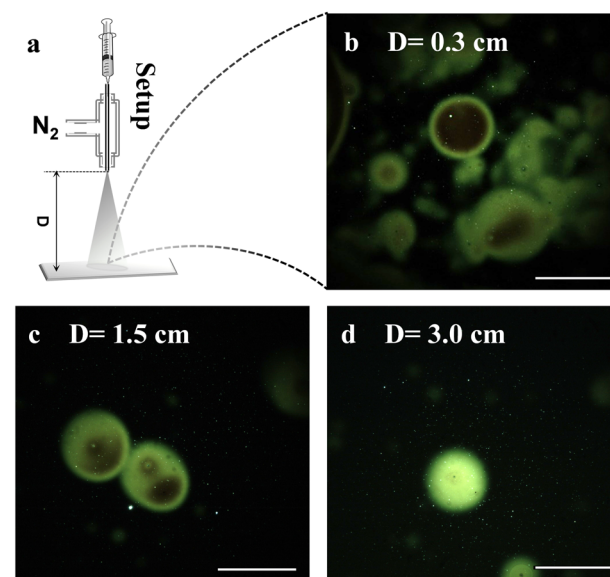

Fig. 2 Effect of the tip-to-deposition surface distance on the distribution of the polymeric R6G solution (100 μM). (a) Schematic diagram of the droplet deposition setup. Fluorescence microscopy images of droplets at a distance of (b) 0.3 cm, (c) 1.5 cm and (d) 3 cm. The scale bar is 100 μm.

At a sufficiently low nebulization gas pressure of 5 psi, the droplets were larger and red-emitting towards the centre and green-emitting towards the periphery (Fig. S5a, ESI†). Similar to the distance effect, we found fluorescence quenching at the core of the droplets. While increasing the gas pressure, the droplet size varied drastically, showing a decrease in the droplet size due to solvent evaporation. An increase in gas pressure from 5 to 20 psi led to a blueshift in the emission and showed green colour (Fig. S5b, ESI†). Only at the highest pressure applied (30 psi), the droplets were fully green (Fig. S5c, ESI†). These observations indicate that the spray parameters of microdroplets significantly influence the aggregation dynamics of the molecules in the droplet.

We have collected hyperspectral fluorescence images of the droplet to understand the extent of aggregation in an individual droplet (Fig. S6a and b, ESI†). The fluorescence spectra collected at and near the surface of the microdroplet reveal that R6G is predominantly monomeric (Fig. S6c and d; Fig. S6b, Locations 1 and 2, ESI†). However, at the interior, majorly R6G is in the polymeric form (Fig. S6e; Fig. S6b, Location 3, ESI†). Interestingly, the gas–liquid interface of the microbubble shows completely monomeric form of the dye (Fig. S6f; Fig. S6b, Location 4, ESI†). We have reported the formation of microbubbles in microdroplets.[19] Herein, the droplet also contains a microbubble, as indicated in Fig. S6a (ESI†). The inner portion of the droplet periphery shows both green and red emissions (Fig. S6d, ESI†). The fluorescence spectrum at the interface of the microbubble shows the presence of only monomeric R6G (Fig. S6f, ESI†). We observed that, as the microbubbles form *in situ* during the flight of microdroplets, the gas–liquid interface could be more dynamic, resulting in such de-aggregation behaviour of the dye molecule.

Fig. 3 correlates the aggregation/de-aggregation properties of R6G at different concentrations between the bulk solution phase, dropcast solid thin film, and imprinted microdroplets. Fig. 3a and b show the bulk phase R6G luminescence under visible and ultraviolet light for five different concentrations: 1 mM, 100 μM, 10 μM, 1 μM, and 100 nM, respectively (Fig. 3(i–v)). Fig. 3c and d show the fluorescence microscopy emission of the dropcast R6G and sprayed sample from a distance of 1.5 cm for five different concentrations. Herein, 1 mM concentration of R6G, the bulk phase as well as the dropcast sample show a red emission. But, in the microdroplets, the emission from the interface is green and that from the core is red. As mentioned earlier, the dull red colour at the core can be attributed to the high-level aggregated nature of R6G and the monomeric nature of R6G at the interface of the microdroplet. Similarly, at 100 μM concentration, the bulk phase and dropcast sample show red emission, whereas microdroplets show green emission at the interface and in the core. As the concentration decreases from 1 mM to 100 μM, the core of the microdroplets shifts from red emission to green because at lower concentrations the microdroplet core can be even more de-aggregated. Therefore, the molecules present in these microdroplets are already monomeric. At 10 μM, bulk droplets themselves show green emission in ultraviolet light. In contrast, the dropcast sample from the
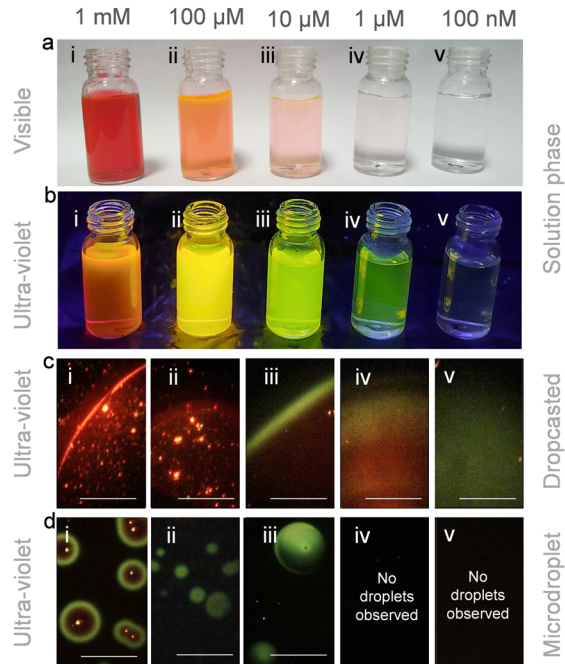

Fig. 3 Concentration effect on aggregation induced emission spectral shift depicted by five different concentrations (1 mM, 100 μM, 10 μM, 1 μM and 100 nM). Bulk phase R6G luminescence under (a) visible light and (b) UV light. (c) Fluorescence images of dropcast R6G and (d) R6G at different concentrations sprayed from a distance of 1.5 cm. The scale bar is 125 μm.

same solution shows both green and red emissions, which signifies the aggregated and monomeric nature of the droplet. The microdroplet of the same shows green emission, irrespective of the core and interface. As the concentration decreases from 10 μM to 1 μM and 100 nM, the emission intensity falls as the concentration of R6G is significantly less. Green emission is much more prominent in the dropcast sample of 100 nM concentration. Microdroplets at 1 μM show complete green colour. Because of extensive dilution, microdroplets corresponding to 100 nM were invisible under a fluorescence microscope. From the above observations, we can conclude that microdroplets regulate aggregation/de-aggregation induced emission shift. At higher concentrations, R6G particles tend to aggregate in the dropcast sample and inside the core of the microdroplet. However, the extent of aggregation is more in the core than in the dropcast sample. Strikingly, even at higher concentrations, particles show monomeric nature at the air–water interface of the microdroplet. For the same concentration, the extent of polymerization of R6G is different in different cases. The microdroplet induces de-aggregation and the dropcast induces aggregation compared to the bulk solution.

We found that the applied potential dramatically affects the aggregation/de-aggregation kinetics of the molecules in microdroplets. The DFM images of droplets containing 100 μM R6G, sprayed at 0 and 4 kV applied potential with a 1.5 cm tip-to-substrate distance, are shown in Fig. S7a and b (ESI†). We observed that droplets at 0 kV show a green interface with a red interior. Droplets at 4 kV were green in colour. It should also be noted that the application of potential causes droplet splitting,
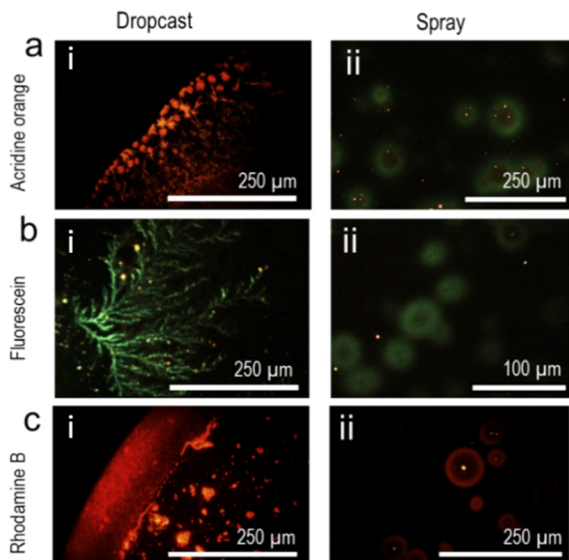
Fig. 4 Fluorescence microscopy images of dropcast *vs.* microdroplets of a few other dye solutions such as (a) acridine orange, (b) fluorescein, and (c) Rhodamine B at 500 μM.

which reduces the size of the droplets and may show a phenomenon similar to the distance effect. Moreover, the smaller the size of the droplets, the higher the surface to volume ratio, due to which de-aggregation is enhanced, resulting in completely green fluorescence (Fig. S5 and S7, ESI†).

The experiments were further extended to other dyes such as acridine orange, fluorescein, and Rhodamine B. The dyes were taken at 500 μM concentrations in water. The fluorescence images of the dropcast thin-film *vs* microdroplets were compared as shown in Fig. 4. A similar phenomenon of de-aggregation was observed for acridine orange. The dropcast image (Fig. 4a(i)) shows bright orange, while the droplet shows a green periphery and dull red interior (Fig. 4a(ii)). The aggregation of fluorescein and Rhodamine B molecules at the core of the microdroplets is evident from fluorescence quenching (Fig. 4b(ii) and c(iii)) which is different from the dropcast sample (Fig. 4b(i) and c(i)). Such aggregation induced quenching of these dye molecules is reported in the earlier literature.[31,32]

In conclusion, we observed that microdroplets assist molecular de-aggregation. Fluorescence microscopy imaging shows that R6G and a few other dye molecules are monomeric in microdroplets than in the solution phase or dropcast solid films. This phenomenon of de-aggregation occurred first at the interface of the droplet, whereas the interior of the droplet still shows aggregation. While the droplets move in the air, the extent of de-aggregation increases until all the molecules become monomeric. We believe that such de-aggregation dynamics at the air/liquid interface helps in overcoming intermolecular interactions and clustering, favouring the chemical reactivity in microdroplets. Such molecular behaviour in droplets could be utilized in understanding prebiotic, cellular and cloud chemistry.

Conflicts of interest

The authors declare no competing financial interest.

References

1 J. Rebek, *Acc. Chem. Res.*, 2009, **42**, 1660–1668.
2 Z. Wei, Y. Li, R. G. Cooks and X. Yan, *Annu. Rev. Phys. Chem.*, 2020, **71**, 31–51.
3 X. Yan, R. M. Bain and R. G. Cooks, *Angew. Chem., Int. Ed.*, 2016, **55**, 12960–12972.
4 J. Kang, S. Lhee, J. K. Lee, R. N. Zare and H. G. Nam, *Sci. Rep.*, 2020, **10**, 1–10.
5 S. Lhee, J. K. Lee, J. Kang, S. Kato, S. Kim, R. N. Zare and H. G. Nam, *Sci. Adv.*, 2020, **6**, eaba0181.
6 A. Gallo Jr., N. H. Musskopf, X. Liu, Z. Yang, J. Petry, P. Zhang, S. Thoroddsen, H. Im and H. Mishra, *Chem. Sci.*, 2022, **13**, 2574–2583.
7 A. Gallo Jr., N. H. Musskopf, X. Liu, Z. Yang, J. Petry, P. Zhang, S. Thoroddsen, H. Im, H. Mishra, C. Zhu, J. S. Francisco, J. K. Lee, H. S. Han, S. Chaikasetsin, D. P. Marron, R. M. Waymouth, F. B. Prinz, R. N. Zare, K. L. Walker, H. S. Han, J. Kang, F. B. Prinz, R. M. Waymouth, H. G. Nam and R. N. Zare, *Proc. Natl. Acad. Sci. U. S. A.*, 2019, **116**, 19222–19224.
8 D. Gao, F. Jin, J. K. Lee and R. N. Zare, *Chem. Sci.*, 2019, **10**, 10974–10978.
9 J. K. Lee, H. S. Han, S. Chaikasetsin, D. P. Marron, R. M. Waymouth, F. B. Prinz and R. N. Zare, *Proc. Natl. Acad. Sci. U. S. A.*, 2020, **117**, 30934–30941.
10 J. K. Lee, K. L. Walker, H. S. Han, J. Kang, F. B. Prinz, R. M. Waymouth, H. G. Nam and R. N. Zare, *Proc. Natl. Acad. Sci. U. S. A.*, 2019, **116**, 19294–19298.
11 C. Zhu and J. S. Francisco, *Proc. Natl. Acad. Sci. U. S. A.*, 2019, **116**, 19222–19224.
12 L. Qiu, Z. Wei, H. Nie and R. G. Cooks, *ChemPlusChem*, 2021, **86**, 2192–6506.
13 N. Narendra, X. Chen, J. Wang, J. Charles, R. G. Cooks and T. Kubis, *J. Phys. Chem. A*, 2020, **124**, 4984–4989.
14 H. Xiong, J. K. Lee, R. N. Zare and W. Min, *J. Phys. Chem. Lett.*, 2020, **11**, 7423–7428.
15 H. Wei, E. P. Vejerano, W. Leng, Q. Huang, M. R. Willner, L. C. Marr and P. J. Vikesland, *Proc. Natl. Acad. Sci. U. S. A.*, 2018, **115**, 7272–7277.
16 P. Basuri, L. E. Gonzalez, N. M. Morato, T. Pradeep and R. G. Cooks, *Chem. Sci.*, 2020, **11**, 12686–12694.
17 B. M. Marsh, K. Iyer and R. G. Cooks, *J. Am. Soc. Mass Spectrom.*, 2019, **30**, 2022–2030.
18 K. Luo, J. Li, Y. Cao, C. Liu, J. Ge, H. Chen and R. N. Zare, *Chem. Sci.*, 2020, **11**, 2558–2565.
19 P. Basuri, A. Chakraborty, T. Ahuja, B. Mondal, J. Shantha Kumar and T. Pradeep, *Chem. Sci.*, 2022, DOI: **10.1039/D2SC04589C**.
20 Z. Arsov, I. Urbančič and J. Štrancar, *Spectrochim. Acta, Part A*, 2018, **190**, 486–493.
21 F. L. Arbeloa, P. R. Ojeda and I. L. Arbeloa, *J. Chem. Soc., Faraday Trans. 2*, 1988, **84**, 1903–1912.
22 R. Vogel, M. Harvey, G. Edwards, P. Meredith, N. Heckenberg, M. Trau and H. Rubinsztein-Dunlop, *Macromolecules*, 2002, **35**, 2063–2070.
23 J. P. Cassidy, J. A. Tan and K. L. Wustholz, *J. Phys. Chem. C*, 2017, **121**, 15610–15618.
24 V. Martínez Martínez, F. López Arbeloa, J. Bañuelos Prieto and I. López Arbeloa, *J. Phys. Chem. B*, 2005, **109**, 7443–7450.
25 O. A. Yeshchenko, I. S. Bondarchuk, V. V. Kozachenko and M. Y. Losytskyy, *J. Lumin.*, 2015, **158**, 294–300.
26 M. Shirakawa, T. Kobayashi and E. Tokunaga, *Appl. Sci.*, 2020, **10**, 3563.
27 O. Valdes-Aguilera and D. C. Neckers, *Acc. Chem. Res.*, 1989, **22**, 171–177.
28 P. Bojarski, A. Matczuk, C. Bojarski, A. Kawski, B. Kukliński, G. Zurkowska and H. Diehl, *Chem. Phys.*, 1996, **210**, 485–499.
29 Y. Bai, P. Luan, Y. Bai, R. N. Zare and J. Ge, *Chem. Sci.*, 2022, **13**, 8341–8348.
30 J. K. Lee, D. Samanta, H. G. Nam and R. N. Zare, *J. Am. Chem. Soc.*, 2019, **141**, 10585–10589.
31 F. L. Arbeloa, P. R. Ojeda and I. L. Arbeloa, *J. Lumin.*, 1989, **44**, 105–112.
32 S. De and R. Kundu, *J. Photochem. Photobiol., A*, 2011, **223**, 71–81.